Climate impacts of intermittent upper ocean mixing induced by tropical cyclones

G. E. Manucharyan,[1] C. M. Brierley,[1] and A. V. Fedorov[1]

Received 17 May 2011; revised 16 August 2011; accepted 17 August 2011; published 29 November 2011.

[1] Tropical cyclones (TC) represent a powerful, albeit highly transient forcing able to redistribute ocean heat content locally. Recent studies suggest that TC-induced ocean mixing can have global climate impacts as well, including changes in poleward heat transport, ocean circulation, and thermal structure. In several previous modeling studies devoted to this problem, the TC mixing was treated as a permanent (constant in time) source of additional vertical diffusion in the upper ocean. In contrast, this study aims to explore the highly intermittent character of the mixing. We present results from a series of coupled climate experiments with different durations of the imposed intermittent mixing but where each has the same annual mean diffusivity. All simulations show robust changes in sea surface temperature and ocean subsurface temperature, independent of the duration of the mixing that varies between the experiments from a few days to a full year. Simulated temperature anomalies are characterized by a cooling in the subtropics, a moderate warming in middle to high latitudes, a pronounced warming of the equatorial cold tongue, and a deepening of the tropical thermocline. These effects are paralleled by substantial changes in ocean and atmosphere circulation and heat transports. While the general patterns of changes remain the same from one experiment to the next, their magnitude depends on the relative duration of the mixing. Stronger mixing, but of a shorter duration, has less of an impact. These results agree with a simple model of heat transfer for the upper ocean with a time-dependent vertical diffusivity.

Citation: Manucharyan, G. E., C. M. Brierley, and A. V. Fedorov (2011), Climate impacts of intermittent upper ocean mixing induced by tropical cyclones, *J. Geophys. Res.*, *116*, C11038, doi:10.1029/2011JC007295.

1. Introduction

[2] Tropical cyclones (TC), also called hurricanes and typhoons, are some of the most destructive weather systems on Earth. Their intense winds cause vigorous ocean vertical mixing [*D'Asaro et al.*, 2007] that brings colder water to the surface while pumping warm surface waters downward. Experiments with ocean models [*Sriver et al.*, 2010] show that strong storms can induce vertical mixing to depths of 250 m and result in a cooling of 6°C or more in the storm's wake. It has been argued that this vertical mixing may have global climate impacts by contributing to oceanic poleward heat transport [*Emanuel*, 2001; *Sriver and Huber*, 2007] and by modifying ocean circulation and thermal structure [*Fedorov et al.*, 2010]. The overarching goal of the present study is to investigate further the climate impacts of this mixing in a comprehensive coupled general circulation model (GCM). Attempts to quantify the amount of TC mixing from observations have found that tropical cyclones induce an annual mean diffusivity in the range of 1 cm^2/s [*Sriver and Huber*, 2007; *Sriver et al.*, 2008] to 6 cm^2/s [*Liu et al.*, 2008]. What effects could this additional mixing have on climate?

[3] Using observed tracks of tropical cyclones and a simplified ocean model, *Emanuel* [2001] estimated that TC-induced mixing contributes 1.4 ± 0.7 PW in ocean poleward heat transport (1 PW = 10^{15} W), which represents a substantial fraction of the observed heat transport by the oceans. He concluded that tropical cyclones might play an important role in driving the ocean thermohaline circulation and thereby regulating climate. *Sriver and Huber* [2007] and *Sriver et al.* [2008] generally supported this conclusion but downgraded heat transport estimates to about 0.3–0.5 PW.

[4] Using an ocean GCM, *Jansen and Ferrari* [2009] demonstrated that an equatorial gap in the TC mixing region altered the structure of the TC-generated heat transports, allowing for a heat convergence toward the equator. On the other hand, *Jansen et al.* [2010] suggested that the climate effects of mixing by TC could be strongly reduced by seasonal factors, namely, by the heat release to the atmosphere in winter (this argument was based on the assumption that the mixing did not penetrate significantly below the seasonal thermocline).

[5] *Hu and Meehl* [2009] investigated the effect of hurricanes on the Atlantic meridional overturning circulation (AMOC) using a relatively coarse global coupled GCM in

[1]Department of Geology and Geophysics, Yale University, New Haven, Connecticut, USA.

Copyright 2011 by the American Geophysical Union.
0148-0227/11/2011JC007295

which tropical cyclones in the Atlantic were included via prescribed winds and precipitation. Their conclusion was that the strength of the AMOC in the model would increase if hurricane winds were taken into account; however, changes in precipitation due to hurricanes would have an opposite effect. More recently, *Scoccimarro et al.* [2011] used a TC-permitting coupled GCM and estimated the contribution of TC to the annually averaged ocean heat transport an order of magnitude smaller than suggested by *Sriver and Huber* [2007] and *Sriver et al.* [2008]. Their model, however, was too coarse to fully resolve tropical storms, leading to the simulated TC activity about 50% weaker with fewer strong storms than are observed.

[6] *Korty et al.* [2008] developed an intermediate-complexity coupled model with a TC parameterization in the form of interactive mixing in the upper ocean that depended on the state of the coupled system. The main aim of the study was to investigate the potential role of tropical cyclones in sustaining equable climates, such as the warm climate of the Eocene epoch. These authors noted a significant increase in TC-induced ocean mixing in a warmer climate, an increase in poleward heat transport, and a corresponding warming of high latitudes.

[7] *Fedorov et al.* [2010] implemented a constant additional mixing within two zonal subtropical bands that they added to the upper ocean vertical diffusivity in a comprehensive climate GCM. They describe a mechanism in which TC warm water parcels are advected by the wind driven circulation and resurface in the eastern equatorial Pacific, warming the equatorial cold tongue by 2°C–3°C, deepening the tropical thermocline, and reducing the zonal SST gradient along the equator. This leads to El Niño-like climate conditions in the Pacific and changes in the atmospheric circulation (the Walker and the Hadley cells). While the goal of this study was to simulate the climate state of the early Pliocene [*Fedorov et al.*, 2006], these results have much broader implications for the role of tropical cyclones in modern climate.

[8] The conclusions of *Fedorov et al.* [2010] generally agree with those of *Sriver and Huber* [2010], who added high-resolution winds from observations to an ocean model, and those of *Pasquero and Emanuel* [2008], who modeled the propagation of oceanic temperature anomalies created by a single instantaneous mixing event. The latter authors found that at least one third of the warm subsurface temperature anomaly was advected by wind-driven circulation toward the equator, which should lead to an increase in ocean heat content in the tropics. In parallel, the impact of small latitudinal variations in background vertical mixing (unrelated to TC) was investigated in a coupled climate model by *Jochum* [2009], who concluded that the equatorial ocean is one of the regions most sensitive to spatial variations in diffusivity.

[9] Several of the aforementioned modeling studies parametrize the effect of tropical storms by adding annual mean values of the TC-induced diffusivity inferred from observations to the background vertical diffusivity already used in an ocean model. However, a single tropical cyclone induces mixing of a few orders of magnitudes greater than the annual mean value. Thus, a question naturally arises: how reliable are results obtained by representing a time-varying mixing with its annual mean value? To that end, the goal of this study is to explore the role of intermittency (i.e., temporal dependence) of the upper ocean mixing in a coupled climate model.

[10] Note that previously, *Boos et al.* [2004] argued that a transient mixing could affect the ocean thermohaline circulation, especially if the mixing was applied near the ocean boundaries. However, their study was performed in an ocean only model with TC mixing penetrating to the bottom of the ocean.

[11] In our study, to mimic the effects of tropical cyclones, we use several representative cases of time-dependent mixing that yield the same annual mean values of vertical diffusivity. The approach remains relatively idealized, in line with the studies of *Jansen and Ferrari* [2009] and *Fedorov et al.* [2010]. A spatially uniform (but time varying) mixing is imposed in zonal bands in the upper ocean. We analyze changes in sea surface temperatures (SST), oceanic thermal structure, the meridional overturning circulation in the ocean and the atmosphere, and poleward heat transports.

[12] In addition, we formulate a simple one-dimensional model of heat transfer to understand the sensitivity of the SST and heat transport to the duration of mixing. It accounts for the gross thermal structure of the upper ocean and incorporates time-dependent coefficients of vertical diffusivity. Using this simple model, we vary the fraction of the year with TC-induced mixing and look at the ocean response. Both the comprehensive and simple models suggest that highly intermittent mixing should generate a response 30%–40% weaker than from a permanent mixing of the same average value.

2. Climate Model and Experiments

[13] We explore the global climate impacts of upper ocean mixing induced by tropical cyclones using the Community Climate System Model, version 3 (CCSM3) [*Collins et al.*, 2006]. The ocean component of CCM3 has 40 vertical levels, a 1.25° zonal resolution, and a varying meridional resolution with a maximum grid size of 1° that reduces to 0.25° in the equatorial region. The atmosphere has 26 vertical levels and a horizontal spectral resolution of T42 (roughly 2.8° × 2.8°). The atmosphere and other components of the model, such as sea ice and land surface, are coupled to the ocean every 24 h.

[14] The conventional vertical mixing of tracers in the ocean model is given by (1) a background diffusivity (0.1 cm^2/s in the upper ocean) attributable to the breaking of internal waves which is constant in time [*Danabasoglu et al.*, 2006] and (2) a diffusivity due to shear instabilities, convection, and double-diffusion processes parameterized by the KPP scheme [*Large et al.*, 1994], which varies in time and space. The annual mean SST and thermal structure of the upper Pacific for this climate model are shown in Figure 1.

[15] To incorporate the effects of tropical cyclones into the model, we add extra vertical diffusivity in the upper ocean within the subtropical bands, defined here as 8°N–40°N and 8°S–40°S (Figure 1). This additional diffusivity can vary with time throughout the year but maintains an annual mean value of 1 cm^2/s (10 times larger than the model's background diffusivity). This mean value, when applied everywhere in the subtropical bands, is probably an overestimation for the present climate; however, TC-induced diffusivity may have been even greater in past warm climates [*Korty et al.*, 2008].

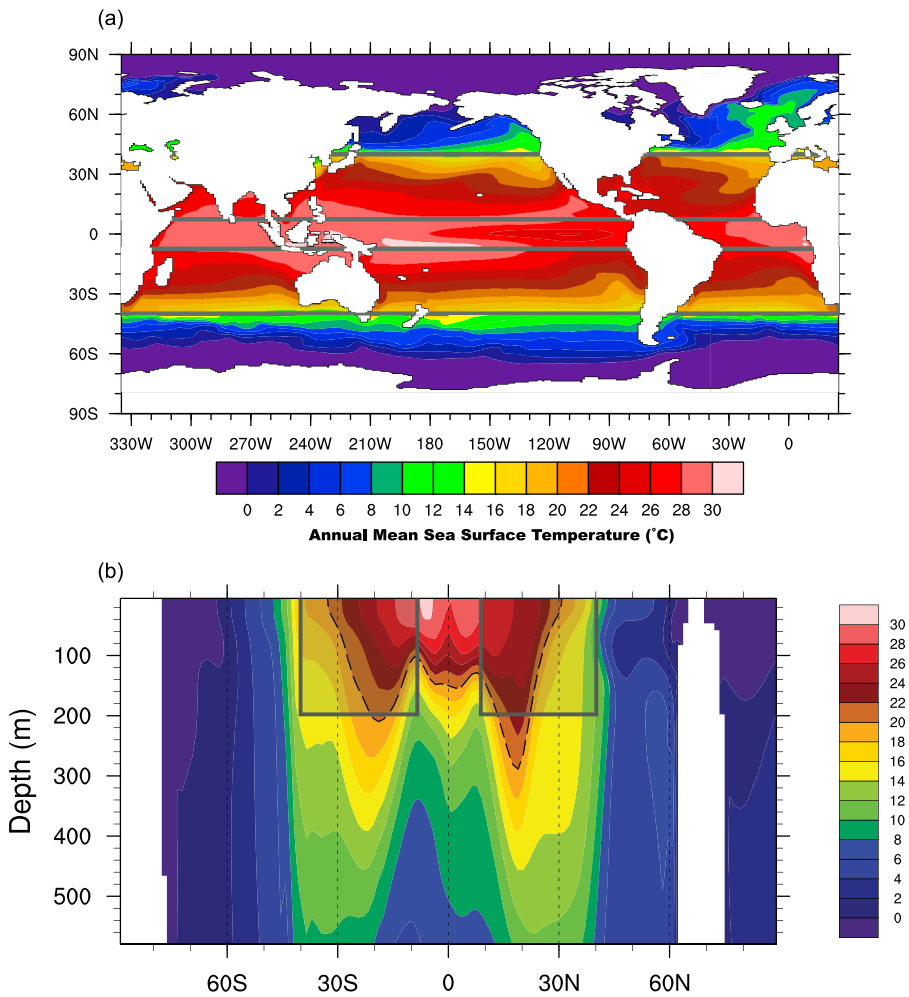

Figure 1. (a) The annual mean sea surface temperature and (b) the upper-ocean temperature along 180°W. Both plots are for the control simulation. In the perturbation experiments, additional mixing is imposed in the zonal bands 8°N–40°N and 8°S–40°S in the upper 200 m of the ocean, as indicated by the shading.

[16] The imposed diffusivity is spatially uniform, following the studies of *Jansen and Ferrari* [2009] and *Fedorov et al.* [2010], who looked at the gross effects of TC mixing in the subtropical bands and neglected zonal variations in the mixing. We ignore buoyancy effects associated with increased precipitation and heat fluxes generated by TC at the ocean surface [*Hu and Meehl*, 2009; *Scoccimarro et al.*, 2011] and focus solely on the mixing effects.

[17] Our choice for the average depth to which TC mixing penetrates is 200 m. In nature, this depth varies significantly depending on the local ocean stratification and the characteristics of a particular storm. Nonetheless, 200 m appears to be a reasonable value for a number of applications. For example, mixing induced by hurricane Frances in the Atlantic penetrated to about 130 m depth, as measured in the hurricane wake by a deployed array of sea floats [*D'Asaro et al.*, 2007]. However, mixing generated by typhoon Kirogi in the Western Pacific may have penetrated to depths of about 500 m with the strongest effects concentrated in the upper 250 m, as estimated from calculations with an ocean GCM forced by observed winds [*Sriver*, 2010]. Using a simple model for TC-induced mixing, *Korty et al.* [2008] estimated the penetration depth at about 200 m for their experiment with moderate concentration of CO_2 in the atmosphere and at 300 m for their warm climate.

[18] We perform four perturbed model experiments with different temporal dependence of TC-induced mixing, and a control run with no additional mixing. In the experiment referred to as "permanent," we specify a diffusivity that remains constant throughout the year. In the other three perturbation experiments the temporal dependence of the mixing is given by step functions alternating between on and off stages. In the "seasonal" experiment a constant mixing is applied only for half a year. In the "single-event" experiment mixing occurs once a year and lasts only 5 days. The "multiple-event" experiment represents six major TC a year that last 2 days each (Figure 2 and Table 1). To take into account the seasonality of tropical cyclone activity, TC mixing in these three experiments is imposed only during the warm part of the year in each hemisphere (summer and fall) with a half year lag between different hemispheres.

[19] We emphasize that in all perturbed cases the annual mean value of TC-induced diffusivity remains the same (1 cm^2/s, similar to that estimated by *Sriver and Huber*

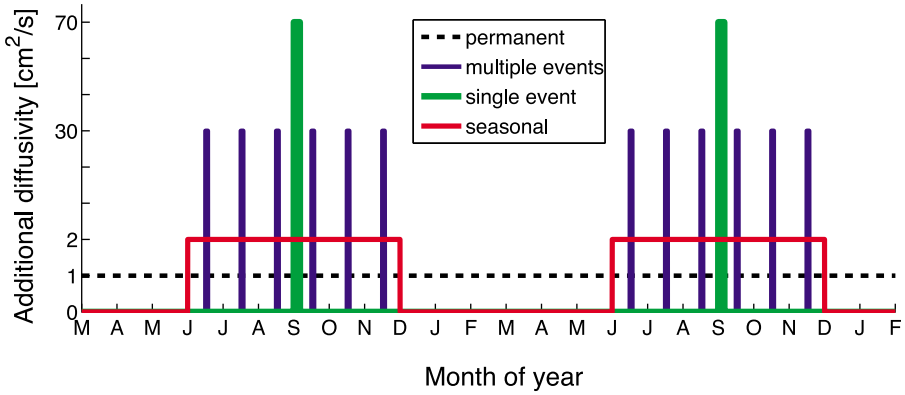

Figure 2. The duration and magnitude of the added vertical diffusivity that replicates TC-induced ocean mixing in different experiments with the climate model (permanent, seasonal, multiple-event, and single-event experiments). The regions where this additional mixing is imposed in perturbation experiments are shown in Figure 1. For further details, see Table 1.

[2007]). Consequently, peak values of the imposed vertical diffusivity for highly intermittent mixing exceed diffusivity for permanent mixing by two orders of magnitude (Table 1).

[20] For each perturbed experiment the model is initialized from a 1000 year simulation with preindustrial conditions and spun up for 200 years after introducing the time-varying vertical diffusivity. Similarly, our control experiment is a 200 year continuation of the preindustrial simulation. The results of the experiments will be presented in terms of anomalies from the control run, averaged over the last 25 years of calculations.

3. Results From the Climate Model

3.1. The Time Scales of Climate Response

[21] We start the discussion of the model results with the time series of several essential climate indexes that show the transient response of the climate system to introduced mixing. The time evolution of global mean temperature and the mean top-of-the-atmosphere (TOA) radiation flux indicates that the climate system is adjusting to changes in the ocean diffusivity with an *e*-folding time scale of nearly 30 years (Figures 3a and 3b). After 100 years these variables do not change, except for weak decadal variations. Initially, we see a drop in global mean temperatures and a counteracting increase in the TOA radiation flux. However, as the TOA radiation imbalance diminishes, the global mean temperature increases and settles at a value slightly greater than in the control run (by 0.1°C–0.2°C). This increase seems to be robust between different experiments, even though its magnitude is comparable with the internal variability of the control run.

[22] Furthermore, the time series of Niño 3.4 index (indicative of the tropical ocean response) show that a warm temperature anomaly of substantial magnitude emerges along the equator also within the first 30 years of simulations (Figure 3c). This indicates that the initial time scales of the climate response are set by the adjustment of the wind-driven circulation and thermal structure of the upper ocean, that occurs on time scales of 20–40 years [*Harper*, 2000; *Barreiro et al.*, 2008] controlled by a combination of advective, wave and diabatic processes [*Boccaletti et al.*, 2004; *Fedorov et al.*, 2004].

[23] In contrast to the first three indexes, the index of the AMOC intensity, related to the deep ocean circulation, shows a sharp decrease after the additional mixing was imposed, but then follows a very slow recovery (Figure 3d). The deep ocean continues its adjustment on longer time scales (centennial to millennial) that should involve diapycnal diffusion throughout the global ocean [*Wunsch and Heimbach*, 2008] and processes in the Southern Ocean [*Haertel and Fedorov*, 2011; *Allison et al.*, 2011].

[24] Nevertheless, roughly after 100 years of simulation, the atmosphere and the upper ocean have gone through their initial adjustment stages and are now experiencing a slow residual climate drift (because of the deep ocean adjustment) as well as decadal variability. We thus focus our discussions on the dynamics of the upper ocean and the atmosphere, but avoid making final conclusions on the state of the AMOC (also see section 5).

Table 1. The Main Characteristics and Results of Different Perturbation Experiments[a]

Mixing Cases	T_{on}	T_{off}	D_{max} (cm^2/s)	OHT (PW)	SST$_b$ (°C)	SST$_{ct}$ (°C)	T_{gm} (°C)	α
Permanent	12 months	0 months	1	0.12	−0.19	2.3	0.11	1.00
Seasonal	6 months	6 months	2	0.21	−0.30	2.2	0.09	0.99
Multiple events	2 days	28 day	30	0.16	−0.14	1.7	0.19	0.72
Single event	5 days	360 days	73	0.13	−0.03	1.7	0.09	0.62

[a]Duration of the imposed mixing (T_{on}, T_{off}), maximum values of the imposed vertical diffusivity (D_{max}), peak anomalies in ocean heat transport (OHT), mean SST cooling within the mixing bands (SST$_b$), the maximum warming of the cold tongue (SST$_{ct}$), anomalies in global mean surface air temperature (T_{gm}), and the regression coefficient (α) for SST anomalies in the transient mixing experiments with respect to those in the permanent mixing run. All properties are the average of the last 25 years of simulation, except the coefficient α, which is the average of the last 100 years.

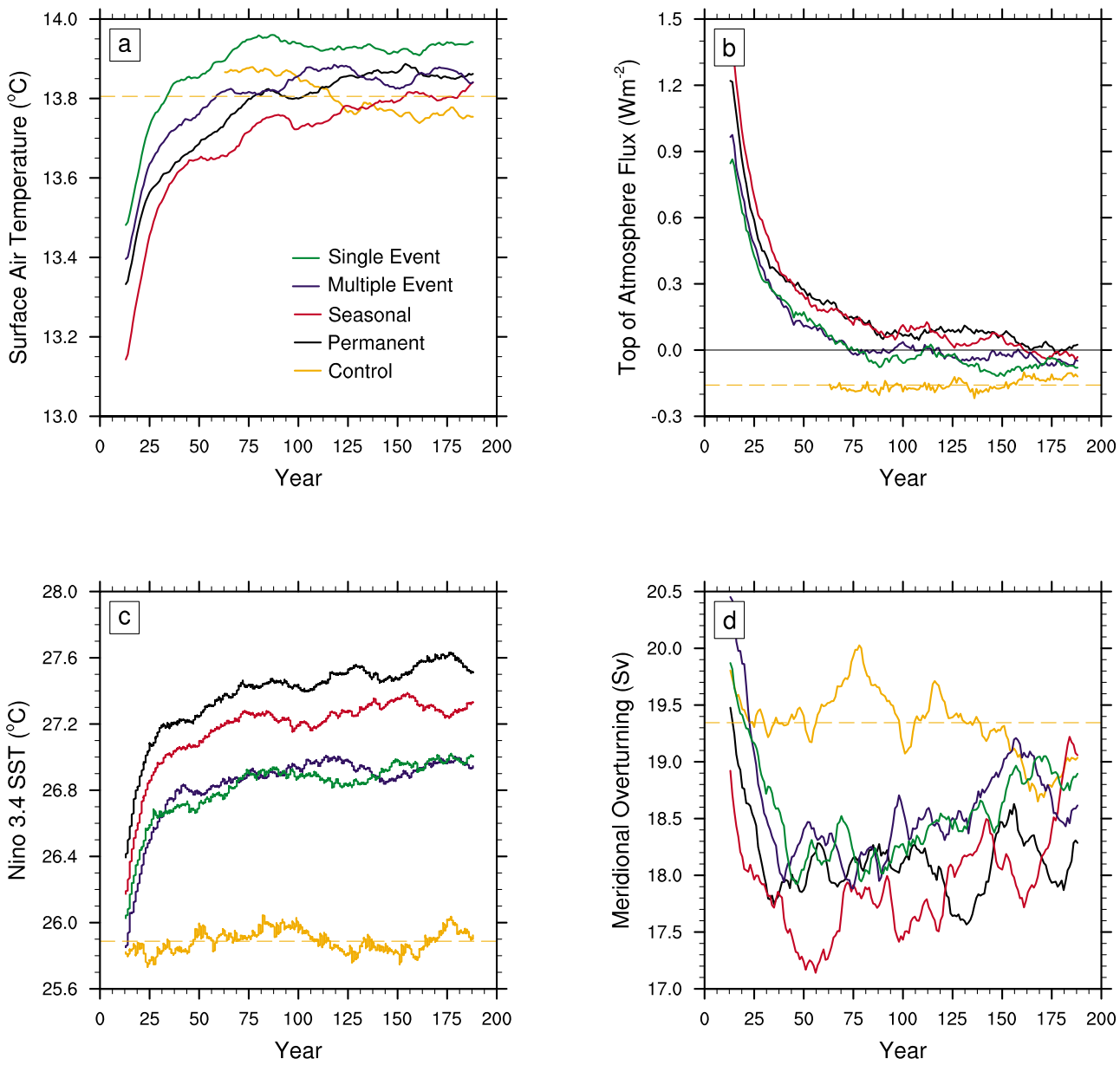

Figure 3. The time evolution of (a) global mean temperature, (b) top-of-the-atmosphere radiation imbalance, (c) the Niño 3.4 SST, and (d) the volume transport of the Atlantic meridional overturning circulation (AMOC) in different experiments, including the control run (orange line), as simulated by the climate model. A 25 year running mean has been applied. Note that the atmospheric data were saved only for the last 150 years of the control simulation.

3.2. Climate Response

[25] All four perturbation experiments produce similar patterns of SST anomalies generated by TC-induced mixing (Figure 4) independent of the exact temporal dependence of the mixing: a weak surface cooling at the location of mixing and a warming in other regions (middle and high latitudes and the equatorial region). The cooling is caused by a greater local entrainment of colder waters from below and pumping of warm surface waters into the interior of the ocean by the additional mixing [*Jansen and Ferrari*, 2009; *Sriver et al.*, 2008; *Sriver and Huber*, 2010]. In turn, the warming is caused by the advection of these relatively warm waters, pumped down by mixing, and their subsequent upwelling to the surface away from the source regions. The warming is amplified by atmospheric feedbacks (see below). The overall pattern of the SST response to the anomalous mixing is similar to that noted in previous works [*Fedorov et al.*, 2010; *Sriver and Huber*, 2010].

[26] The largest SST cooling in the mixing bands is achieved for the seasonal experiment with an average reduction of 0.3°C and local values reaching 1°C (Figure 4). Seasonal mixing causes a stronger SST change than the permanent mixing, because vertical mixing is more efficient in modifying the SSTs during summer, when the thermal stratification

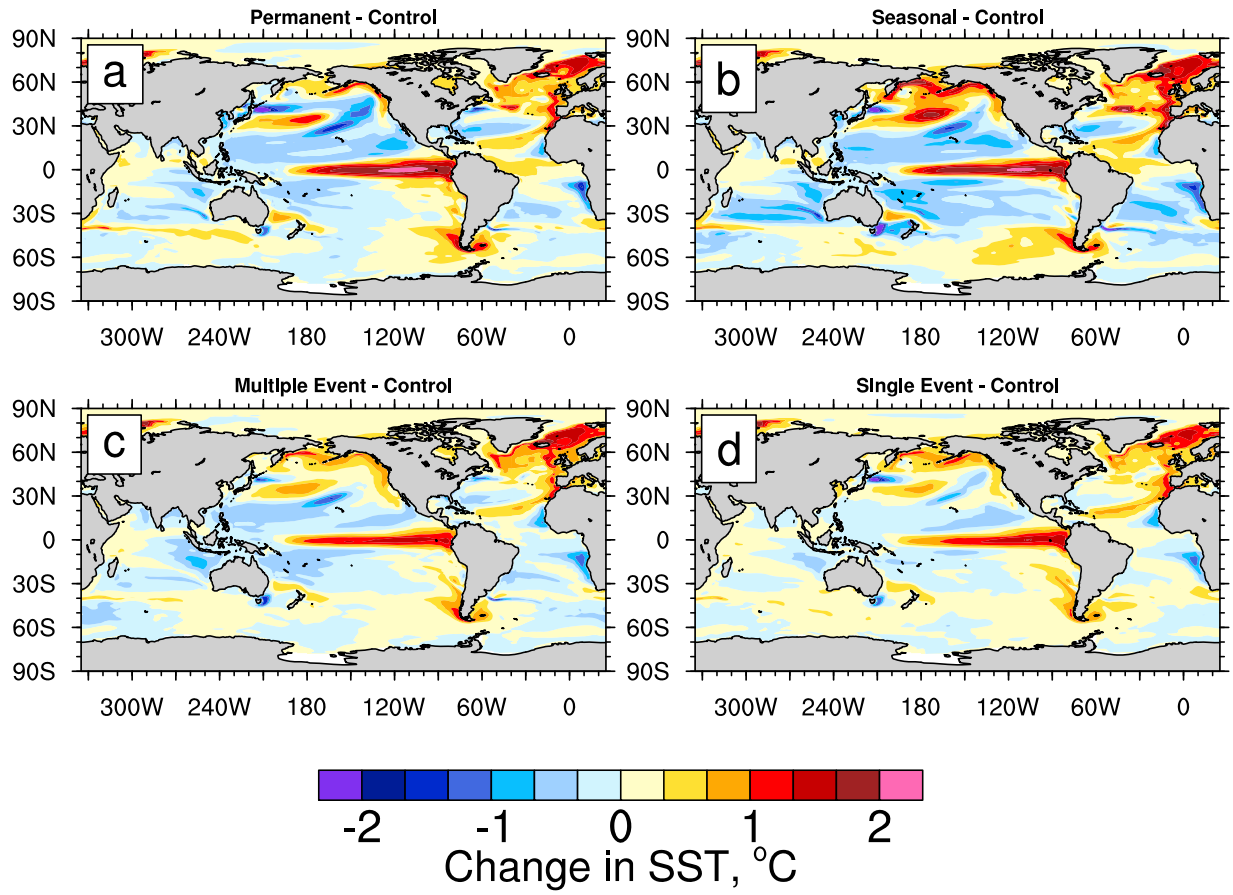

Figure 4. Sea surface temperature anomalies in the four different perturbation experiments with added ocean vertical diffusivity in the subtropical bands: permanent, seasonal, multiple-event, and single-event experiments. Anomalies are calculated with respect to the control run and averaged over the last 25 years of calculations.

is stronger and surface waters are warmer. In contrast, during winter mixed layers are deep and surface waters are relatively cold, which makes it more difficult to modify SSTs by additional mixing. The magnitude of cooling for the permanent mixing experiment is 0.2°C on average and decreases slightly as the mixing becomes highly intermittent (Table 1).

[27] Perhaps, the most pronounced feature of these experiments is the warming of the cold tongue in the eastern equatorial Pacific that can reach magnitudes over 2°C. In the permanent and seasonal experiments the warming has similar strengths with a slightly weaker warming in the single- and multiple-event experiments. The cold tongue warming is amplified by the weakening of the Walker cell (not shown) via the Bjerknes feedback [*Bjerknes*, 1969] and a corresponding reduction in the thermocline slope along the equator (Figure 5).

[28] The additional mixing is restricted to a depth of 200 m, yet, temperature anomalies are seen as deep as 500 m (Figure 5). The warm surface waters, pumped down by TC mixing, are advected by the wind-driven ocean circulation as well as diffusing downward by the unaltered deep background mixing. The subsurface temperature signal is again strongest for the seasonal and the permanent mixing experiments with temperature anomalies reaching magnitudes of 5°C–10°C. The spatial structure of the anomalies is similar for all the mixing cases and is characterized by a deepening of the tropical thermocline (Figure 5).

3.3. Correlation Between Different Experiments

[29] We observe that spatial patterns of the climatological anomalies bear strong similarities between different model runs. This brings us back to the question of how good is the approximation of intermittent mixing with its annual mean. To address this question, we choose the permanent mixing run as the reference case, and compare it to the runs with intermittent mixing with the aim of quantifying the differences and similarities between the cases.

[30] As a representative field for our analysis we use the global spatial pattern of SST anomalies. We choose this particular field as it couples the ocean and the atmosphere and reflects changes occurring in both fluids. At any particular instant in time, the magnitudes of vertical mixing are different in each run, and so are the SSTs. Therefore, we compare time-averaged anomalies, defined here through 25 year running means.

[31] We find that SST anomalies for the intermittent mixing runs are well correlated with anomalies for the permanent mixing run, with correlation coefficients remaining higher than 0.8 throughout the whole integration (Figure 6a).

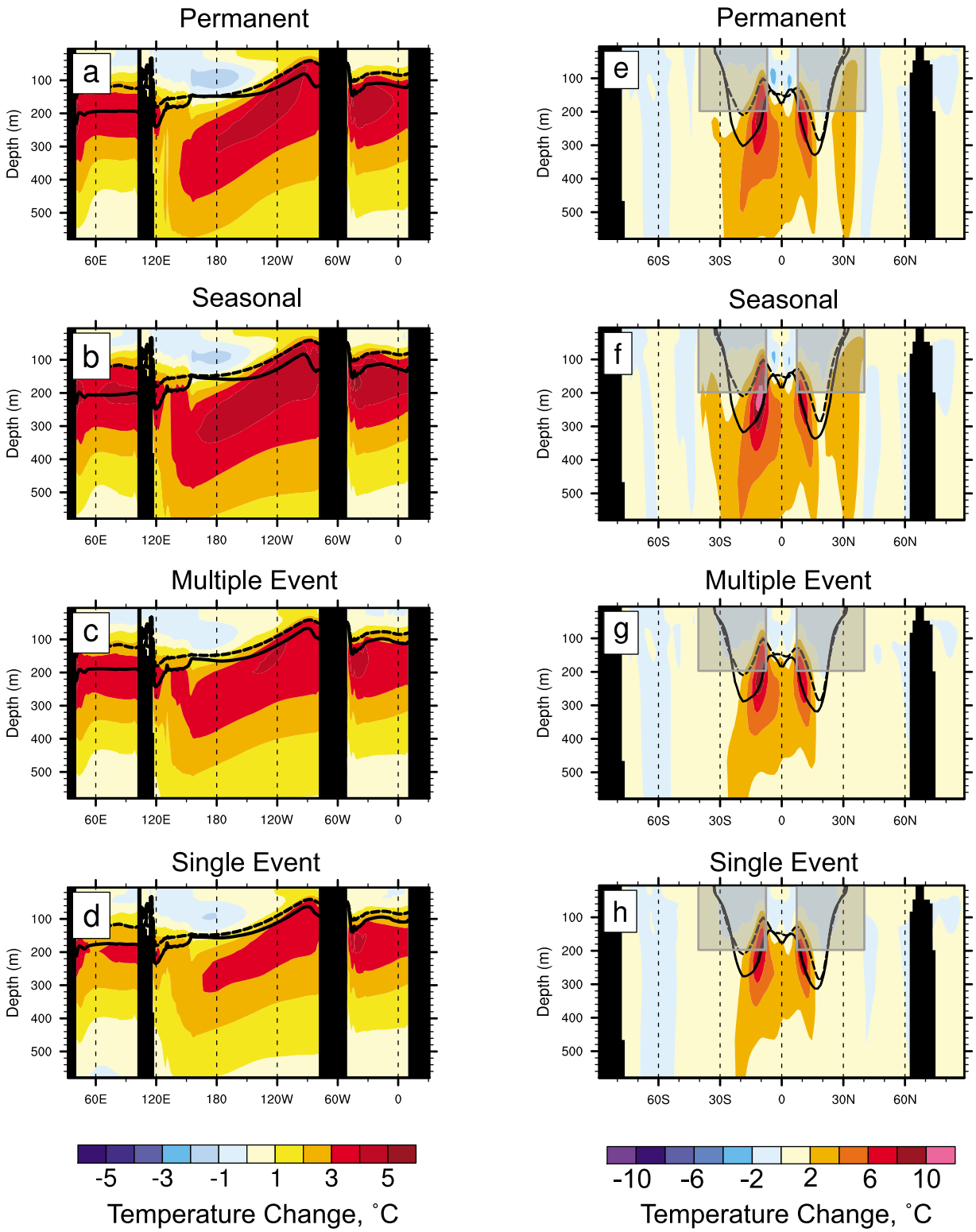

Figure 5. Ocean temperature anomalies as a function of depth (a–d) along the equator and (e–h) along 180°W for different perturbation experiments. From top to bottom: permanent, seasonal, multiple-event, and single-event experiments. The solid and dashed black lines denote the position of the 20°C isotherm (a proxy for the tropical thermocline depth) in the perturbation experiments and the control run, respectively. Note the deepening of the tropical thermocline, the reduction of the thermocline slope along the equator, and the strong subsurface temperature anomalies that extend to depths of about 500 m. Ocean diffusivity is modified in the upper 200 m in the subtropical bands, 8°N–40°N and 8°S–40°S (regions shaded gray). Anomalies are calculated with respect to the control run and averaged over the last 25 years of calculations.

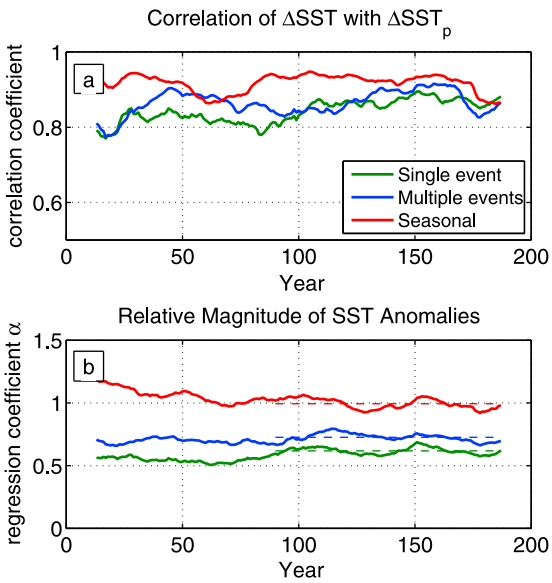

Figure 6. (a) Temporal changes of the correlation coefficients computed between annual mean SST anomalies in the transient mixing experiments and those in the permanent mixing run. (b) The same as in Figure 6a, but for the regression coefficient α. These coefficients indicate how close to each other the SST anomalies in different experiments are.

Although all the runs experience a climate drift as well as low-frequency variability, these variations occur in a correlated way. Furthermore, the correlation coefficients have no negative trends, implying that decorrelation time scale between different runs (if decorrelation does occur) is much longer than the 200 year integration time.

[32] The fact that the spatial fields are well correlated, allows us to calculate the relative magnitudes of SST anomalies in the intermittent mixing experiments with respect to SST anomalies for permanent mixing. We assume the following relation between SST anomalies for each run:

$$\Delta\mathrm{SST} = \alpha\Delta\mathrm{SST}_{\mathrm{perm}} + err, \tag{1}$$

where $\Delta\mathrm{SST}$ and $\Delta\mathrm{SST}_{\mathrm{perm}}$ are SST anomalies for different intermittent mixing runs and for the permanent mixing run, respectively, α is the relative magnitude of the anomaly, and *err* is the error of such approximation. The regression coefficient α is computed as

$$\alpha = \frac{\langle \Delta\mathrm{SST}\ \Delta\mathrm{SST}_{\mathrm{perm}} \rangle}{\langle \Delta\mathrm{SST}_{\mathrm{perm}} \Delta\mathrm{SST}_{\mathrm{perm}} \rangle}, \tag{2}$$

where the operator $\langle\ \rangle$ denotes a dot product between the two fields (weighted by the surface area). When computing these coefficients we actually subtract the means (relatively small) from the SST anomalies. Obviously, for the permanent mixing experiment, $\alpha = 1$ and $err \equiv 0$. For the intermittent mixing experiments, α shows the relative magnitude of SST anomalies with respect to the permanent mixing run.

[33] These coefficients stay relatively constant in time after the initial adjustment period (Figure 6b), which allows us to evaluate the relative magnitude of SST anomalies in different experiments. Accordingly, anomalies in the seasonal experiment have almost the same magnitude as the permanent case ($\alpha \approx 1$). The multiple-event and single-event experiments show relative magnitudes of 72% and 62%, respectively, over the last 100 years (Table 1). The root-mean-square error of such a representation lies between 0.2°C–0.3°C for the

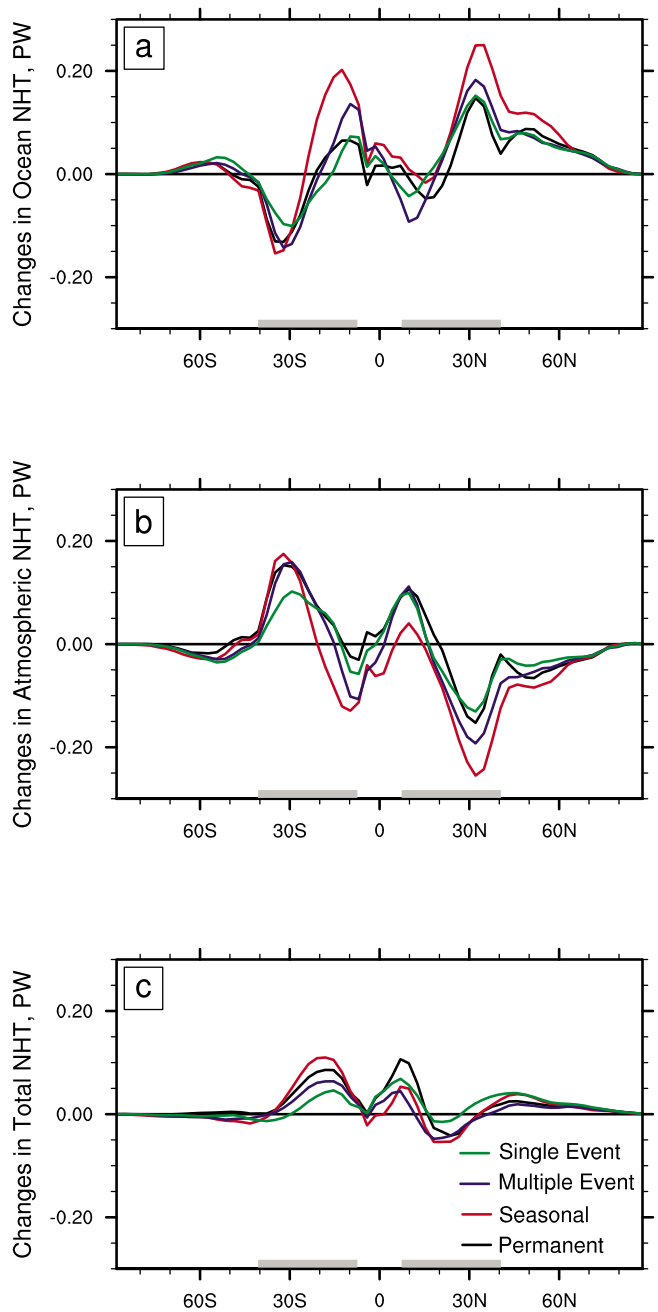

Figure 7. Anomalous northward heat transport (NHT) by (a) the ocean, (b) the atmosphere, and (c) the entire ocean-atmosphere system for different perturbation experiments. Thick gray lines on the horizontal axis indicate the latitudinal extent of the regions with enhanced mixing; the magnitude of decadal changes in the heat transports does not exceed 0.05 PW.

whole duration of the experiments, which implies that approximating the gross effects of intermittent mixing with appropriately scaled permanent mixing will produce a relatively small error (which is a factor of 2 or 3 smaller than the natural decadal variability of SST anomalies).

3.4. Oceanic and Atmospheric Overturning Circulations and Heat Transports

[34] Changes in ocean temperatures are paralleled by anomalies in surface heat fluxes and hence in ocean poleward heat transport (Figure 7). The ocean heat uptake increases in the regions of additional mixing, which results in two major effects: a stronger ocean heat transport to middle and high latitudes (as suggested by *Emanuel* [2001]) and anomalous heat convergence toward the equator (as noted by *Jansen and Ferrari* [2009] and *Fedorov et al.* [2010]). The strongest ocean heat transport anomalies are produced by seasonal mixing; it is harder to distinguish between the other cases because of decadal variability. The peak anomalous heat transport by the ocean reaches 0.15–0.25 PW, which roughly matches the estimates by *Sriver and Huber* [2007].

[35] The observed increase in ocean heat transport is largely due to changes in the amount of heat transported by the shallow wind-driven circulation, rather than the deep overturning circulation. In fact, we observe an initial weakening of the AMOC (Figure 3d) possibly caused by the surface warming of the Norwegian sea (Figure 4) which has a stabilizing effect on convection. However, the integration time of our experiments is not sufficient to reach an equilibrium, and at the end of 200 year simulation the AMOC still exhibits a trend toward higher values. Whether the AMOC eventually returns to its undisturbed strength, or perhaps intensifies in agreement with the hypothesis of *Emanuel* [2001], is unclear. A definite answer to this question will require several thousand years of calculations.

[36] It is important that SST changes, specifically an increase in the meridional temperature gradient between the subtropics and the equatorial region, cause the intensification of the atmospheric Hadley circulation (Figure 8). As a result, anomalies in oceanic heat transport are partially compensated by the atmosphere (Figure 7) in a manner reminiscent of Bjerknes compensation [*Bjerknes*, 1964; *Shaffrey and Sutton*, 2006]. For example, whereas the ocean carries more heat toward the equator, the stronger Hadley circulation transports more heat away from the equator. Consequently, changes in oceanic heat transport of nearly 0.3 PW do not necessarily represent changes in the total heat transport by the system (Figure 7c), which stays below 0.1 PW.

[37] Nevertheless, a substantial fraction of oceanic heat transport remains uncompensated as a stronger poleward heat transport by the ocean induces the atmospheric water vapor feedback in mid to high latitudes and a decrease in global albedo related to changes in low clouds and/or sea ice [*Herweijer et al.*, 2005]. Such changes result in a slight increase of global mean temperature (0.1°C–0.2°C) in all the experiments with enhanced mixing (Table 1).

[38] Finally, one of the consequences of the stronger winds associated with the more intense Hadley circulation is the strengthening of the ocean shallow overturning circulation, i.e., the subtropical cells (STC) in Figure 8. This strengthening of the STC appears to moderate the warming of the equatorial cold tongue but is not able to reverse ocean heat convergence toward the equator.

4. A Simple Model for the Upper Ocean Thermal Structure With TC Mixing

4.1. Formulation of the Model

[39] To investigate further the ocean sensitivity to intermittent mixing, here we formulate a simple one-dimensional model describing the gross thermal structure of the upper ocean when subjected to anomalous mixing events. The model equations for the vertical temperature profile in the subtropical ocean $T = T(z, t)$ are as follows:

$$T_t = (\kappa T_z)_z - \gamma(T - T^*), \tag{3a}$$

$$\kappa T_z = -\alpha_s(T - T_s),\ z = 0, \tag{3b}$$

$$\kappa T_z = \alpha_b(T - T_b),\ z = -H. \tag{3c}$$

[40] This is a heat transfer equation with horizontal advection parameterized as a restoring term, $-\gamma(T - T^*)$. The restoring time scale, γ^{-1} = 10 year, is chosen to represent advection by the wind-driven subtropical cell (STC) in the Pacific. The upstream temperature profile T^* is obtained as a steady state solution of equation (1) with a constant background diffusivity, κ_0, and no advective restoring. Thus, the restoring profile T^* is also a steady state solution of the full system, which will be used as the background profile to compare solutions corresponding to different forms of intermittent mixing. In the coupled climate model both the strength of the circulation and the upstream profile change a little in response to the additional mixing, but we will neglect such effects here.

[41] Atmospheric heat fluxes at the ocean surface are parameterized by restoring the surface temperature to a prescribed atmospheric temperature, T_s (30°C). At the bottom of the integration domain (H = 300 m), the temperature is restored to a deep ocean temperature, T_d (10°C), which is set by the deep ocean circulation. The restoring time scales (or piston velocities [e.g., *Griffies et al.*, 2005]) are α_s^{-1} = 0.3 m/d at the surface and α_d^{-1} = 0.08 m/d at the bottom of the domain. These values are chosen in such a way that a surface temperature anomaly caused by a mixing event would be restored roughly within two weeks and temperature anomalies at the bottom of the domain within two months (in terms of e-folding time scales).

[42] The time-dependent vertical diffusivity consists of two components: a background diffusivity, κ_0 (0.1 cm^2/s) and an intermittent diffusivity, $\kappa'(t)$, replicating the effect of TC (with the annual mean value of 1 cm^2/s above 200 m, zero below). For simplicity, we neglect the seasonal cycle and restrict the form of $\kappa'(t)$ to a periodic step function with an on/off behavior:

$$\kappa'(t+\tau) = \kappa'(t) = \begin{cases} \kappa_{\text{on}}, & 0 < t \le r\tau, \\ 0, & r\tau < t \le \tau. \end{cases} \tag{4}$$

The period, τ, of the TC-induced diffusivity is chosen to be 1 year, yielding one event per year. The parameter r is a measure of the mixing intermittency; it indicates the fraction

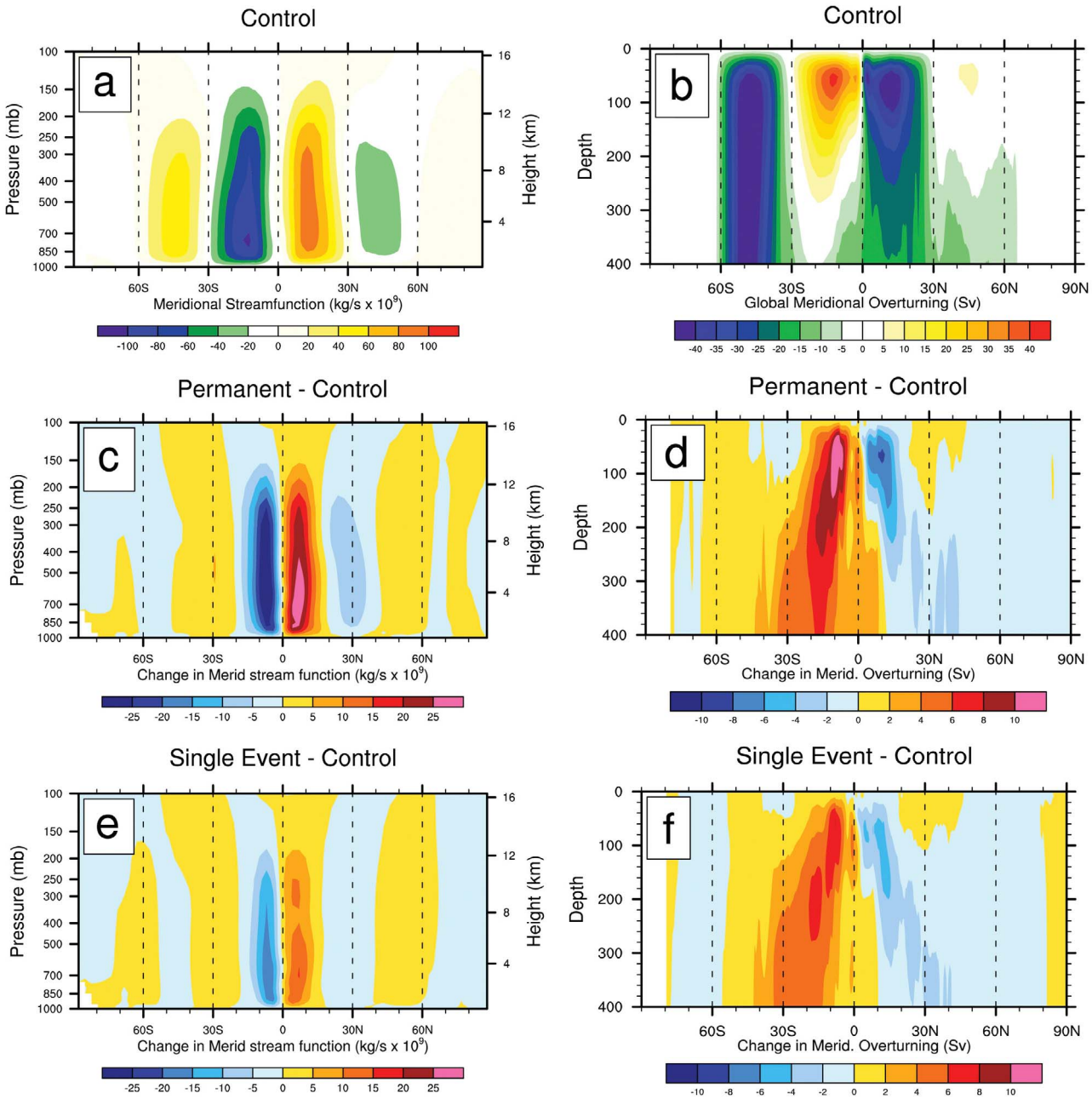

Figure 8. (a, b) The zonally averaged atmospheric and oceanic circulations in the control run (the Hadley cells and the ocean shallow subtropical cells, respectively) and their anomalies in the (c, d) permanent mixing and (e, f) single-event experiments. Note the strengthening of both the atmospheric and shallow oceanic meridional overturning cells. Anomalies are averaged over the last 25 years of calculations.

of the year that the TC mixing is on. Note that additional vertical diffusivity during the on stage (κ_{on}) is normalized by r, so that the annual mean diffusivity stays constant for all experiments.

[43] The parameter r provides a link to the coupled model simulations, in which $r = 1$ for the permanent case, $r = 0.5$ for the seasonal, and $r = 0.01$ for the single-event case (the multiple-event case does not have a direct analogue in this framework). The model is integrated numerically for a broad range of parameter r (between 0.003 and 1) using a finite difference scheme with a vertical resolution of 5 m and an adaptive time step. Each experiment lasts for 200 years to match the coupled model experiments and to insure that statistical properties of this system are equilibrated.

4.2. Idealized Model Results

[44] The steady state solution of equation (3) without additional diffusion describes an ocean with a linearly decreasing temperature (Figure 9a, dashed line). Adding permanent diffusivity ($r = 1$) in the upper 200 m leads to a substantial cooling at the surface and a warming at depth (Figure 9a, solid black line). Note, that warm anomalies penetrate to depths below

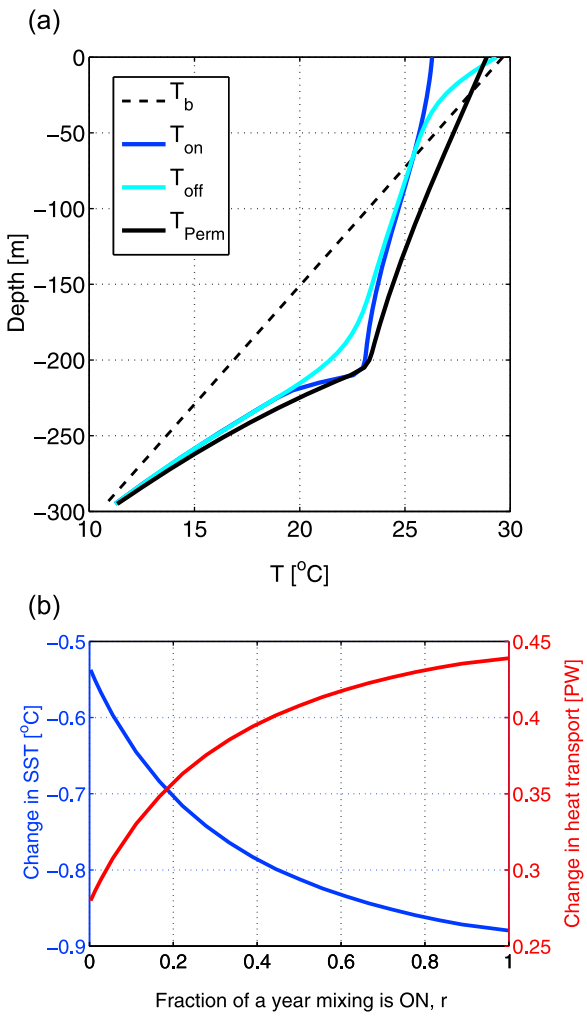

Figure 9. (a) Temperature profiles as a function of depth obtained as solutions of the simple one-dimensional model with no additional mixing (dashed line) and with the addition of permanent mixing (solid black line). For comparison, also shown are temperature profiles for an experiment with $r = 0.05$ directly after the mixing event (dark blue line) and after the restoring period (light blue line). (b) Anomalies in surface temperature and implied ocean heat transport estimated from the simple model for different values of the parameter r. The mean value of the imposed diffusivity (1 cm^2/s) remains the same for all r.

200 m where no additional mixing is applied. This is a result of slow diffusion due to the model original background diffusivity. The penetration depth (L_p) is dictated by the balance between vertical diffusion and advective restoring with the following scaling: $L_p \sim \sqrt{\kappa_0/\gamma}$. This gives a penetration depth of 170 m below the additional mixing, which is in rough agreement with the climate model, where strong temperature anomalies are observed at depths of 400–500 m.

[45] When the additional diffusivity varies with time ($r < 1$), so does the temperature profile. During the interval when the transient mixing is on, the temperature profile becomes more uniform with depth (Figure 9a, dark blue line). However, during the off stage this profile gradually relaxes toward the undisturbed temperature distribution (Figure 9a, light blue line). Thus, the intermittent mixing causes large oscillations in ocean temperature. When averaged, these oscillations produce persistent cold anomalies at the ocean surface and warm anomalies at depth. The horizontal advection of these warm subsurface temperature anomalies generates anomalous heat transport (ΔHF), which eventually leads to the warming in the equatorial cold tongue and of middle and high latitudes.

[46] The largest SST cooling (ΔSST) is achieved for constant TC mixing ($r = 1$). As the mixing becomes more intermittent ($r < 1$), the magnitude of the SST change decreases (Figure 9b, blue line). In the limit of very small r (highly intermittent mixing), the average SST anomaly is reduced roughly by 30%–40%, but nevertheless remains significant; that is, short but strong mixing events are indeed important. The magnitude of the anomalous heat transport follows roughly the same dependence on r (Figure 9b, red line).

[47] Overall, such behavior is consistent with the coupled model, implying that TC-induced climate changes are directly related to thermal anomalies generated locally by TC mixing. The magnitude of the changes depends on how intermittent the mixing is, but only to a moderate extent. Both the simple and coupled climate models suggest that parameterizations of TC as a source of permanent mixing may lead to an overestimation of climate impacts of tropical cyclones, but will have the correct spatial pattern.

5. Discussions and Conclusions

[48] This study investigates the global climate impacts of temporally variable upper ocean mixing induced by tropical cyclones using a global ocean-atmosphere coupled model and a simple heat transfer model of the upper ocean. The time-averaged temperature anomalies in the coupled model show robust spatial patterns in response to additional vertical mixing. Specifically, we observe a weak surface cooling at the location of the mixing (~0.3°C), a strong warming of the equatorial cold tongue (~2°C), and a moderate warming in middle to high latitudes (0.5°C–1°C). We also observe a deepening of the tropical thermocline with subsurface temperature anomalies extending to 500 m. These and other changes, summarized in Table 1, are consistent between the different experiments.

[49] Additional mixing leads to an enhanced oceanic heat transport (on the order of 0.2 PW) from the regions of increased mixing toward high latitudes and the equatorial region. This effect is partially compensated by the atmosphere, resulting in smaller changes in the total heat transport. An increase of the ocean poleward heat transport agrees with the original idea of *Emanuel* [2001]. However, it is largely due to the transport by the wind-driven, rather than the thermohaline, circulation. There is also a small increase in global mean temperature (~0.2°C), associated with the greater ocean heat transport (for a discussion, see *Herweijer et al.* [2005]).

[50] The magnitude of the climate response to enhanced mixing depends not only on the time-averaged value of the added diffusivity, but also on its temporal dependence. In our coupled climate model, a single-event mixing produces a roughly 40% weaker response than permanent mixing (with the same annual mean diffusivity). This result is reproduced

by our simple one-dimensional heat transfer model for the upper ocean with a time-dependent vertical diffusivity. The simple model shows a similar reduction of the local SST anomaly and the anomalous heat transport from the mixing region when we decrease the fraction of the year with mixing.

[51] The presence of the seasonal cycle in the coupled model amplifies the impact of tropical cyclones as they occur during summer, when warm surface temperatures are favorable for pumping heat into the interior of the ocean. In our coupled model this effect apparently overcomes the effect of seasonality described by *Jansen et al.* [2010], who emphasized heat release from the ocean back to the atmosphere during winter that could weaken ocean thermal anomalies. Their mechanism appears to be more important for relatively weak cyclones generating shallow mixing, and not for stronger cyclones that contribute to the mixing most.

[52] To address the issue of the model dependency of our conclusions we performed several additional experiments with the Community Earth System Model (CESM), which is a newer version of the model that we used initially (CCSM3). Important differences between the models include the implementation of the near surface eddy flux parameterization [*Ferrari et al.*, 2008; *Danabasoglu et al.*, 2008] and a new sea ice component in CESM. Also, we used a lower-resolution version of the new model as compared to CCSM3. The results of the new experiments are very similar to the prior experiments, showing the equatorial warming and the deepening of the thermocline, the cooling of the subtropical bands, and the strengthening of the shallow overturning circulation in the ocean and the Hadley cells in the atmosphere. The patterns of generated climatological SST anomalies remain well correlated between different mixing runs, with highly intermittent mixing having a somewhat weaker response. The only major difference concerns the AMOC behavior and SST changes in the high-latitude northern Atlantic; in the new model the AMOC intensity does not change in response to additional mixing. The persistent warming of the Norwegian Sea, observed in CCSM, is replaced by a surface cooling balanced by a density compensating freshwater anomaly. These effects are probably due to the new sea ice model or the lower model resolution; the question of their robustness goes beyond the scope of the present paper.

[53] The consistent spatial patterns of the climate response to transient mixing suggest that in coupled climate simulations a highly intermittent upper ocean mixing can be represented by adding permanent or constant seasonal mixing, perhaps rescaled appropriately.

[54] Several other relevant questions remain beyond the scope of this study, including the role of spatial variations of the TC-induced mixing and the adiabatic effects of their cyclonic winds on oceanic circulation through Ekman upwelling. It is also feasible that for present-day climate our results actually give the upper bound on the climate response to tropical cyclones. A critical issue is the average depth of mixing penetration; choosing a depth significantly shallower than 200 m for the experiments would dampen the overall signal. Restricting the zonal extent of the mixing bands in each ocean basin, more in line with observations, would also reduce the signal.

[55] Ultimately, simulations with TC-resolving climate models will be necessary to fully understand the role of tropical cyclones in climate. However, the current generation of GCMs are only slowly approaching this limit and are still unable to reproduce many characteristics of the observed hurricanes, especially of the strongest storms critical for the ocean mixing [e.g., *Gualdi et al.*, 2008; *Scoccimarro et al.*, 2011; P. L. Vidale, personal communication, 2011].

[56] **Acknowledgments.** This research was supported in part by grants from NSF (OCE0901921), Department of Energy Office of Science (DE-FG02-08ER64590), and the David and Lucile Packard Foundation. Resources of the National Energy Research Scientific Computing Center supported by the DOE under contract DE-AC02-05CH11231 are also acknowledged. We thank K. Emanuel and two anonymous reviewers for helpful comments and suggestions.

References

Allison, L., H. Johnson, and D. Marshall (2011), Spin-up and adjustment of the Antarctic Circumpolar Current and global pycnocline, *J. Mar. Res.*, in press.

Barreiro, M., A. Fedorov, R. Pacanowski, and S. Philander (2008), Abrupt climate changes: How freshening of the Northern Atlantic affects the thermohaline and wind-driven oceanic circulations, *Annu. Rev. Earth Planet. Sci.*, *36*, 33–58.

Bjerknes, J. (1964), Atlantic air-sea interaction, *Adv. Geophys.*, *10*(1), 1–82.

Bjerknes, J. (1969), Atmospheric teleconnections from the equatorial Pacific, *Mon. Weather Rev.*, *97*(3), 163–172.

Boccaletti, G., R. Pacanowski, S. Philander, and A. Fedorov (2004), The thermal structure of the upper ocean, *J. Phys. Oceanogr.*, *34*(4), 888–902.

Boos, W., J. Scott, and K. Emanuel, (2004), Transient diapycnal mixing and the meridional overturning circulation, *J. Phys. Oceanogr.*, *34*(1), 334–341.

Collins, W., et al. (2006), The Community Climate System Model version 3 (CCSM3), *J. Clim.*, *19*, 2122–2143.

Danabasoglu, G., W. G. Large, J. J. Tribbia, P. R. Gent, B. P. Briegleb, and J. C. McWilliams (2006), Diurnal coupling in the tropical oceans of CCSM3, *J. Clim.*, *19*, 2347–2365.

Danabasoglu, G., R. Ferrari, and J. McWilliams (2008), Sensitivity of an ocean general circulation model to a parameterization of near-surface eddy fluxes, *J. Clim.*, *21*, 1192–1208.

D'Asaro, E., T. Sanford, P. Niiler, and E. Terrill (2007), Cold wake of Hurricane Frances, *Geophys. Res. Lett.*, *34*, L15609, doi:10.1029/2007GL030160.

Emanuel, K. (2001), Contribution of tropical cyclones to meridional heat transport by the oceans, *J. Geophys. Res.*, *106*, 14,771–14,781.

Fedorov, A., R. Pacanowski, S. Philander, and G. Boccaletti (2004), The effect of salinity on the wind-driven circulation and the thermal structure of the upper ocean, *J. Phys. Oceanogr.*, *34*(9), 1949–1966.

Fedorov, A., P. Dekens, M. McCarthy, A. Ravelo, P. DeMenocal, M. Barreiro, R. Pacanowski, and S. Philander (2006), The Pliocene paradox (mechanisms for a permanent El Nino), *Science*, *312*(5779), 1485–1489.

Fedorov, A., C. Brierley, and K. Emanuel (2010), Tropical cyclones and permanent El Niño in the early Pliocene epoch, *Nature*, *463*, 1066–1070.

Ferrari, R., J. McWilliams, V. Canuto, and M. Dubovikov (2008), Parameterization of eddy fluxes near oceanic boundaries, *J. Clim.*, *21*, 2770–2789.

Griffies, S., et al. (2005), Formulation of an ocean model for global climate simulations, *Ocean Sci.*, *1*(1), 45–79.

Gualdi, S., et al. (2008), Changes in tropical cyclone activity due to global warming: Results from a high-resolution coupled general circulation model, *J. Clim.*, *21*, 5204–5228.

Haertel, P., and A. Fedorov (2011), The ventilated ocean, *J. Phys. Oceanogr.*, doi:10.1175/2011JPO4590.1, in press.

Harper, S. (2000), Thermocline ventilation and pathways of tropical-subtropical water mass exchange, *Tellus, Ser. A*, *52*(3), 330–345.

Herweijer, C., R. Seager, M. Winton, and A. Clement (2005), Why ocean heat transport warms the global mean climate, *Tellus, Ser. A*, *57*(4), 662–675.

Hu, A., and G. Meehl (2009), Effect of the Atlantic hurricanes on the oceanic meridional overturning circulation and heat transport, *Geophys. Res. Lett.*, *36*, L03702, doi:10.1029/2008GL036680.

Jansen, M., and R. Ferrari (2009), Impact of the latitudinal distribution of tropical cyclones on ocean heat transport, *Geophys. Res. Lett.*, *36*, L06604, doi:10.1029/2008GL036796.

Jansen, M., R. Ferrari, and T. Mooring (2010), Seasonal versus permanent thermocline warming by tropical cyclones, *Geophys. Res. Lett.*, *37*, L03602, doi:10.1029/2009GL041808.

Jochum, M. (2009), Impact of latitudinal variations in vertical diffusivity on climate simulations, *J. Geophys. Res.*, *114*, C01010, doi:10.1029/2008JC005030.

Korty, R., K. Emanuel, and J. Scott (2008), Tropical cyclone-induced upper-ocean mixing and climate: Application to equable climates, *J. Clim.*, *21*, 638–654.

Large, W., J. McWilliams, and S. Doney (1994), Oceanic vertical mixing: A review and a model with a nonlocal boundary layer parameterization, *Rev. Geophys.*, *32*(4), 363–403.

Liu, L., W. Wang, and R. Huang (2008), The mechanical energy input to the ocean induced by tropical cyclones, *J. Phys. Oceanogr.*, *38*(6), 1253–1266.

Pasquero, C., and K. Emanuel (2008), Tropical cyclones and transient upper-ocean warming, *J. Clim.*, *21*, 149–162.

Scoccimarro, E., S. Gualdi, A. Bellucci, A. Sanna, P. G. Fogli, E. Manzini, M. Vichi, P. Oddo, and A. Navarra (2011), Effects of tropical cyclones on ocean heat transport in a high resolution coupled general circulation model, *J. Clim*, *24*, 4368–4384.

Shaffrey, L., and R. Sutton (2006), Bjerknes compensation and the decadal variability of the energy transports in a coupled climate model, *J. Clim.*, *19*, 1167–1181.

Sriver, R. L. (2010), Climate change: Tropical cyclones in the mix, *Nature*, *463*, 1032–1033.

Sriver, R. L., and M. Huber (2007), Observational evidence for an ocean heat pump induced by tropical cyclones, *Nature*, *447*, 577–580.

Sriver, R. L., and M. Huber (2010), Modeled sensitivity of upper thermocline properties to tropical cyclone winds and possible feedbacks on the Hadley circulation, *Geophys. Res. Lett.*, *37*, L08704, doi:10.1029/2010GL042836.

Sriver, R. L., M. Huber, and J. Nusbaumer (2008), Investigating tropical cyclone-climate feedbacks using the TRMM Microwave Imager and the Quick Scatterometer, *Geochem. Geophys. Geosyst.*, *9*, Q09V11, doi:10.1029/2007GC001842.

Sriver, R. L., M. Goes, M. E. Mann, and K. Keller (2010), Climate response to tropical cyclone-induced ocean mixing in an Earth system model of intermediate complexity, *J. Geophys. Res.*, *115*, C10042, doi:10.1029/2010JC006106.

Wunsch, C., and P. Heimbach (2008), How long to oceanic tracer and proxy equilibrium?, *Quat. Sci. Rev.*, *27*(7–8), 637–651.

C. M. Brierley, A. V. Fedorov, and G. E. Manucharyan, Department of Geology and Geophysics, Yale University, Kline Geology Laboratory, PO Box 208109, 210 Whitney Ave., New Haven, CT 06511, USA. (christopher.brierley@yale.edu; alexey.fedorov@yale.edu; georgy.manucharyan@yale.edu)